PAPER • OPEN ACCESS

Friction anomalies at first-order transition spinodals: 1T-TaS$_2$

To cite this article: Emanuele Panizon *et al* 2018 *New J. Phys.* **20** 023033

View the article online for updates and enhancements.

Related content

New Journal of Physics

The open access journal at the forefront of physics

PAPER

CrossMark

Friction anomalies at first-order transition spinodals: 1T-TaS$_2$

Emanuele Panizon[1], Torben Marx[2], Dirk Dietzel[2] , Franco Pellegrini[1], Giuseppe E Santoro[1,3,4], Andre Schirmeisen[2,5] and Erio Tosatti[1,3,4,5]

[1] International School for Advanced Studies (SISSA), Via Bonomea 265, I-34136 Trieste, Italy
[2] Institute of Applied Physics, Justus-Liebig-University Giessen, Heinrich-Buff-Ring 16, D-35392 Giessen, Germany
[3] CNR-IOM Democritos National Laboratory, Via Bonomea 265, I-34136 Trieste, Italy
[4] The Abdus Salam International Centre for Theoretical Physics (ICTP), Strada Costiera 11, I-34151 Trieste, Italy
[5] Authors to whom any correspondence should be addressed

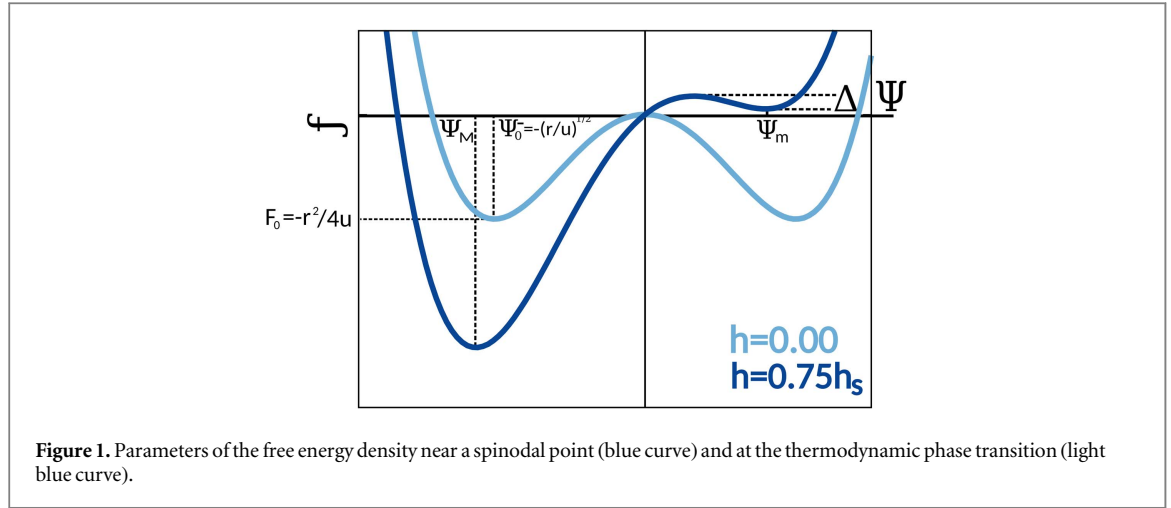**E-mail:** schirmeisen@ap.physik.uni-giessen.de and tosatti@sissa.it

Abstract

Revealing phase transitions of solids through mechanical anomalies in the friction of nanotips sliding on their surfaces, a successful approach for continuous transitions, is still an unexplored tool for first-order ones. Owing to slow nucleation, first-order structural transformations occur with hysteresis, comprised between two spinodal temperatures where, on both sides of the thermodynamic transition, one or the other metastable free energy branches terminates. The spinodal transformation, a collective one-shot event without heat capacity anomaly, is easy to trigger by a weak external perturbation. Here we show that even the gossamer mechanical action of an AFM-tip can locally act as a trigger, narrowly preempting the spontaneous spinodal transformation, and making it observable as a nanofrictional anomaly. Confirming this expectation, the CCDW–NCCDW first-order transition of the important layer compound 1T-TaS$_2$ is shown to provide a demonstration of this effect.

Introduction

Revealing and understanding solid state phase transitions through nanomechanical and nanofrictional effects at their surfaces is an unconventional upcoming approach. Friction of nanosized tips on dry solid surfaces can be seen as a kind of 'Braille spectroscopy'—reading the physics underneath by touching [1]. At second-order structural phase transitions, critical fluctuations give indeed rise to surface dissipation anomalies, as predicted [2] and observed in non-contact atomic force microscope friction on SrTiO$_3$ [3], providing additional important understanding about the underlying mechanism. Another non-structural example is the drop of electronic friction, observed upon cooling a metal below the superconducting Tc in correspondence to the opening of the BCS gap [4].

Unlike these established examples, a vast majority of solid state structural and electronic phase transitions is however of discontinuous, first-order type. Since at a first-order transition two free energy branches cross without criticality, might not its frictional signature just consist of some unpredictable and unremarkable jump? This scenario is, we show here, unduly pessimistic. In fact, not one but two frictional anomalies will occur at a first-order transition, at the two hysteresis end-point temperatures. While hysteresis depends on kinetics, its maximal width is determined by the loss of local stability. The hysteresis end-point are close in character to spinodal—the point where the metastable state stability is lost and the transformation is collective [5]. At the spinodal temperatures, on both sides of the thermodynamic first-order transition, there should be a dissipation peak in the response of the AFM/friction force microscope (FFM) as the tip moves on, sweeping in the course of time newer and newer surface areas where the near-spinodal transformation can be 'harvested'. These predictions are first argued theoretically and then demonstrated experimentally in the important layer compound 1T-TaS$_2$.

In this layer compound a well known first-order, hysteretic transition of joint structural and electronic nature takes place between a low-temperature commensurate charge-density-wave (CCDW) $\sqrt{13} \times \sqrt{13}$

Figure 1. Parameters of the free energy density near a spinodal point (blue curve) and at the thermodynamic phase transition (light blue curve).

phase, [6, 7] believed to be Mott insulating [8, 9], and a nearly commensurate charge-density-wave (NCCDW) phase, metallic and even superconducting under pressure [7] and alloying with 1T-TaSe$_2$ [10]. Notably, 1T-TaS$_2$ has been subject to very intense studies over the last decade, in connection with transient or hidden metastable phases under high excitation, [11–13] with the unusual substrate, thickness, and disorder dependence of its transitions [14–17], and with a spin liquid in the CCDW phase [18–20].

While insensitive to these electronic excitations, the present frictional study sheds fresh light on the thermodynamic nature of the important CCDW–NCCDW transformation.

Theoretical model

Model and methods

Beginning with theory, we adopt the simplest mean-field Landau–Ginzburg–Wilson [21] or Cahn–Allen [22] approach, which works reasonably well for many structural transitions. Assume the schematic model bulk solid free energy density

$$f[\Psi] = -\frac{r}{2}\Psi^2(\boldsymbol{\rho}) + \frac{u}{4}\Psi^4(\boldsymbol{\rho}) + \frac{J}{2}(\nabla\Psi)^2 + h(\boldsymbol{\rho})\Psi(\boldsymbol{\rho}), \tag{1}$$

(where r, u, J are positive parameters) governing the evolution of a generic, non-conserved real order parameter Ψ supposed to represent collectively all mechanically relevant thermodynamic variables, as a function of the spatial coordinate $\boldsymbol{\rho}$ (in this schematic outline, we provisionally ignore the distinction between surface and bulk). The external field h includes here a uniform term describing the free energy imbalance between the two minima at negative and positive Ψ(h thus represents here the temperature deviation from the first-order thermodynamic transition point) plus a localized mechanical perturbation representing the tip which, when moving in the course of time, will undergo mechanical dissipation, observable as friction. In the spatially uniform field and perturbation-free case $(\nabla\Psi)^2 = 0, h = 0$, two equivalent free energy minima $F_0 = -r^2/4u$ occur at $\Psi_0^{\pm} = \pm\sqrt{r/u}$ identifying the two phases. A first-order transition occurs between them when a growing uniform h causes Ψ to switch from initially positive to negative or vice versa. The transition can occur at or near the free energy crossing point $h = 0$ only through nucleation, that would allow the thermal crossing of the large free energy barrier between the two nearly equivalent states. Nucleation, however, is an especially slow process for structural transitions, where therefore a $\Psi > 0$ metastable state often persists up to large positive fields h. Upon reversing the field, the $\Psi < 0$ state will similarly persist for negative h, giving rise to hysteresis. The maximum theoretical width of the hysteresis cycle is determined by the two *spinodal* points $h_s = \pm 2r^{3/2}/3^{3/2}u^{1/2}$, where the transformation must necessarily happen because the metastable free energy minimum disappears, as sketched in figure 1. At the two spinodal points $\Psi_s = \pm\sqrt{r/3u}$ and $f_s = (1/12)r^2/u$ the transformation occurs collectively rather than locally, as amply described in literature, reviewed in a different context in [5].

A spinodal point is associated with the collective dynamics of all macroscopic variables accompanying the first-order transition including structure, volume, conductivity, etc. When that point is approached, even a small perturbation can locally overcome the marginal free energy barrier and trigger a large-scale transformation from the metastable to the stable state, as pictured in figure 2(a). If that perturbation is provided by a sliding tip at the crystal surface, the small but finite triggering work will show up as a burst in the tip's measured frictional dissipation. Moreover, as the tip moves forward on the surface, it can convert newer and newer patches from
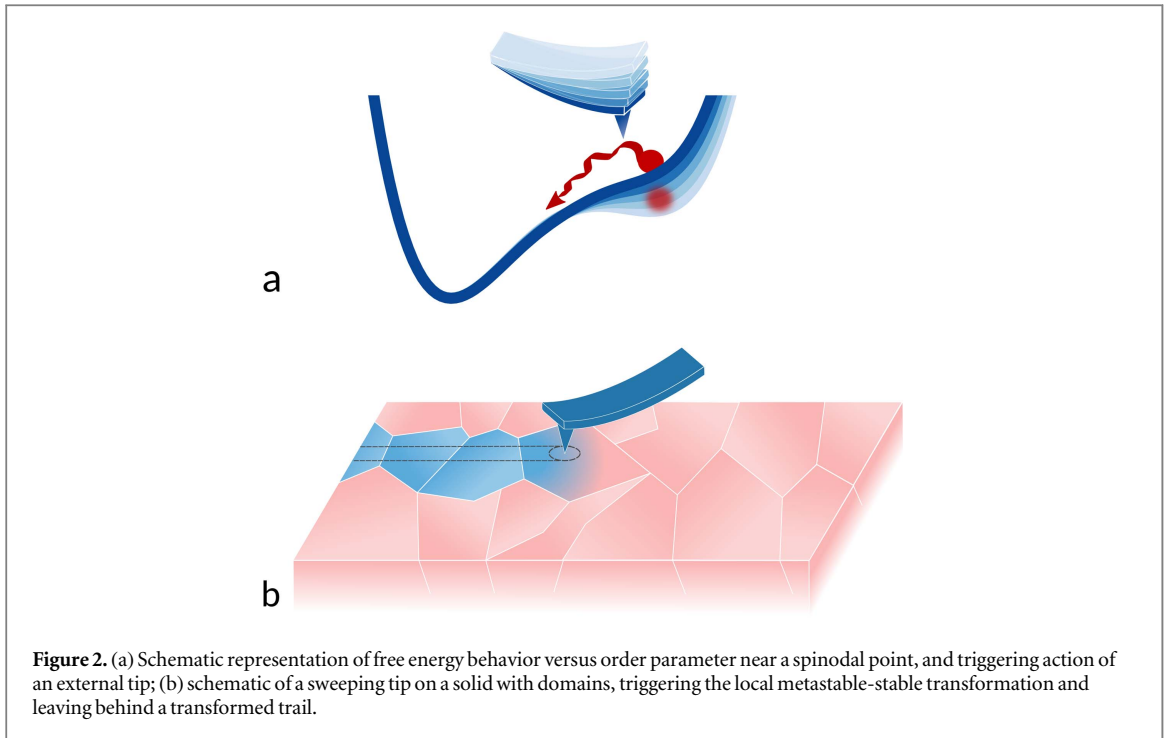
Figure 2. (a) Schematic representation of free energy behavior versus order parameter near a spinodal point, and triggering action of an external tip; (b) schematic of a sweeping tip on a solid with domains, triggering the local metastable-stable transformation and leaving behind a transformed trail.
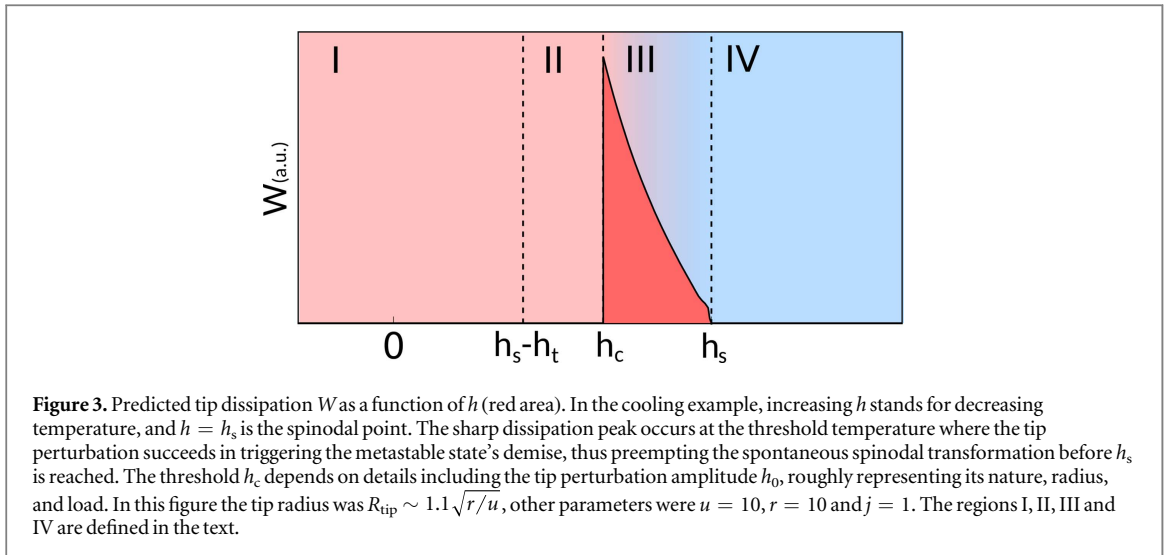
metastable to stable, figure 2(b). The pursuit of the frictional consequences of a first-order transition close to its spinodal points is our goal.

To calculate numerically the nucleation processes involved in the dissipation we employed a variational method. As in classical nucleation theory, we are interested in describing a system forced to evolve from $\Psi = \Psi_M$ at $\rho = 0$, to $\Psi = \Psi_m$ at $\rho = \infty$, ρ being the radial distance between the center of nucleation. To represent this behavior, trial functions are constructed as $\Psi(\rho) = \Psi_m + (\Psi_M - \Psi_m)/2 \tanh((\rho - R_0)/\gamma)$, where R_0 is the radius of the droplet and γ its interface width. We consider, in a semi-infinite 3D system, the nucleation energy $F[\rho; R_0, \gamma]$, which depends variationally on the two parameters R_0 and γ. For each R_0 we use a gradient descent algorithm to minimize in respect to γ, and then we maximize for R_0 to find the nucleation barrier F_0. Based on that we can numerically calculate the homogeneous nucleation radius R_c and its corresponding barrier. The numerical solutions have been constructed for values of ρ in an interval $[0, 30]$ divided in a mesh of $N = 500$ points, which was sufficient to enforce convergence. The values of R_c where inside the interval range of ρ for all values of h.

Theoretical results

Starting with $\Psi > 0$, and turning up the uniform field (i.e., approaching from above the real system spinodal temperature on cooling down) $h \rightarrow h_s$, we observe that $f[\Psi]$ is a local minimum—a metastable state—protected by a marginal barrier Δ which disappears at the spinodal point $h = h_s$, figure 1. Before that point is reached, in the metastable state, a weak additional local perturbation $\delta h(\rho)$ such as that of a static nano-tip imparts to the state variable Ψ a destabilizing modification, whose effect, initially small, grows as the spinodal point is approached. Moreover if the tip moves in space with velocity **v**, so that $\delta h_{tip}(\boldsymbol{\rho}, t) = h_0(\boldsymbol{\rho} - \mathbf{v}t)$, then it may or it may not succeed to locally trigger the spinodal transformation. If it does, then some mechanical work will be spent, and that expense will reflect in the form of a burst in the tip's mechanical dissipation.

Four different frictional regimes, shown in figure 3, are crossed as a function of h (i.e., of temperature)—when evolving for example from a high temperature metastable state Ψ_m to a low-temperature stable state Ψ_M on cooling. In regime (I), h is still far from the spinodal point h_s, the free energy barrier protecting the metastable state is substantial, the tip perturbation too weak to push the system above it, and the tip friction is unaffected. In a second regime (II), the tip may succeed to 'wet' its surrounding with a small converted nucleus Ψ_M of radius R_{tip}, yet still unable to overcome the nucleation barrier if $R_{tip} < R_c$, the effective inhomogeneous nucleation critical radius. Depending whether this nucleus does or does not reconvert back to Ψ_m as the tip moves on, there will or will not be frictional work. Assuming reconversion (for slow tip motion), the friction is again zero, and the transformed nucleus is carried along adiabatically by the tip. In regime (III), attained as h increases, the nucleation radius eventually shrinks below the tip perturbation radius, $R_c < R_{tip}$. The system suddenly overcomes the barrier as in figure 2 (a), thus provoking the irreversible transformation $\Psi_m \rightarrow \Psi_M$ extending in principle out to infinite distance—in practice, out to some macroscopically determined radius L defined by the

Figure 3. Predicted tip dissipation W as a function of h (red area). In the cooling example, increasing h stands for decreasing temperature, and $h = h_s$ is the spinodal point. The sharp dissipation peak occurs at the threshold temperature where the tip perturbation succeeds in triggering the metastable state's demise, thus preempting the spontaneous spinodal transformation before h_s is reached. The threshold h_c depends on details including the tip perturbation amplitude h_0, roughly representing its nature, radius, and load. In this figure the tip radius was $R_{tip} \sim 1.1\sqrt{r/u}$, other parameters were $u = 10$, $r = 10$ and $j = 1$. The regions I, II, III and IV are defined in the text.

sample quality, defects, and morphology. At this threshold temperature the mean tip frictional dissipation suddenly jumps from zero to finite, thereafter decreasing smoothly and eventually vanishing when the true spinodal point $h \to h_s$ is reached, and dissipation again disappears, regime (IV). Our mean-field model predicts the frictional dissipation burst in the shape shown figure 3, a behavior which we now describe before seeking an experimental demonstration.

Let us consider the nucleation energy profile $F[\boldsymbol{\rho}]$ without tip, i.e. $\delta h_{tip} = 0$, as calculated before. Now add to $F[\boldsymbol{\rho}]$ the tip perturbation $h_{tip}(\boldsymbol{\rho}) = h_0 \Theta(\|\boldsymbol{\rho} - \mathbf{x}_{tip}\| - R_{tip})$ whose effect is to lower the local barrier as sketched in figure 2(a). At $h = h_c$, a value which depends on the tip perturbation magnitude h_0, the nucleation radius becomes smaller than the wetting radius $R_c < R_{tip}$, the local nucleation barrier disappears and the massive transformation is triggered. The tip will spend at that point the triggering work $W = F_0$. This work, as mentioned, is paid only once, because after conversion the stable phase Ψ_M extends macroscopically away, and the system becomes subsequently insensitive to the tip. It should be stressed here therefore that, unlike second-order transitions between equilibrium states, which take place reversibly as the temperature is cycled across the critical point, the spinodal transformation takes place only once as the spinodal point is first crossed (unless the system is, as it were, 'recharged'). In a real system actually the size of the transformed region is limited by defects to some average radius L determined by, e.g., grain boundaries, steps, etc, so that newer and newer metastable surface areas can be 'harvested' in the course of time, as sketched in figure 2(b). The tip moving with velocity v will explore fresh untransformed metastable regions with a rate $\mu \sim v/L$, figure 2(b), therefore dissipating a frictional power $P = W\mu = F_0 v/L$, a quantity which is non-zero in the temperature range corresponding to $h_c < h < h_s$ as depicted in figure 3.
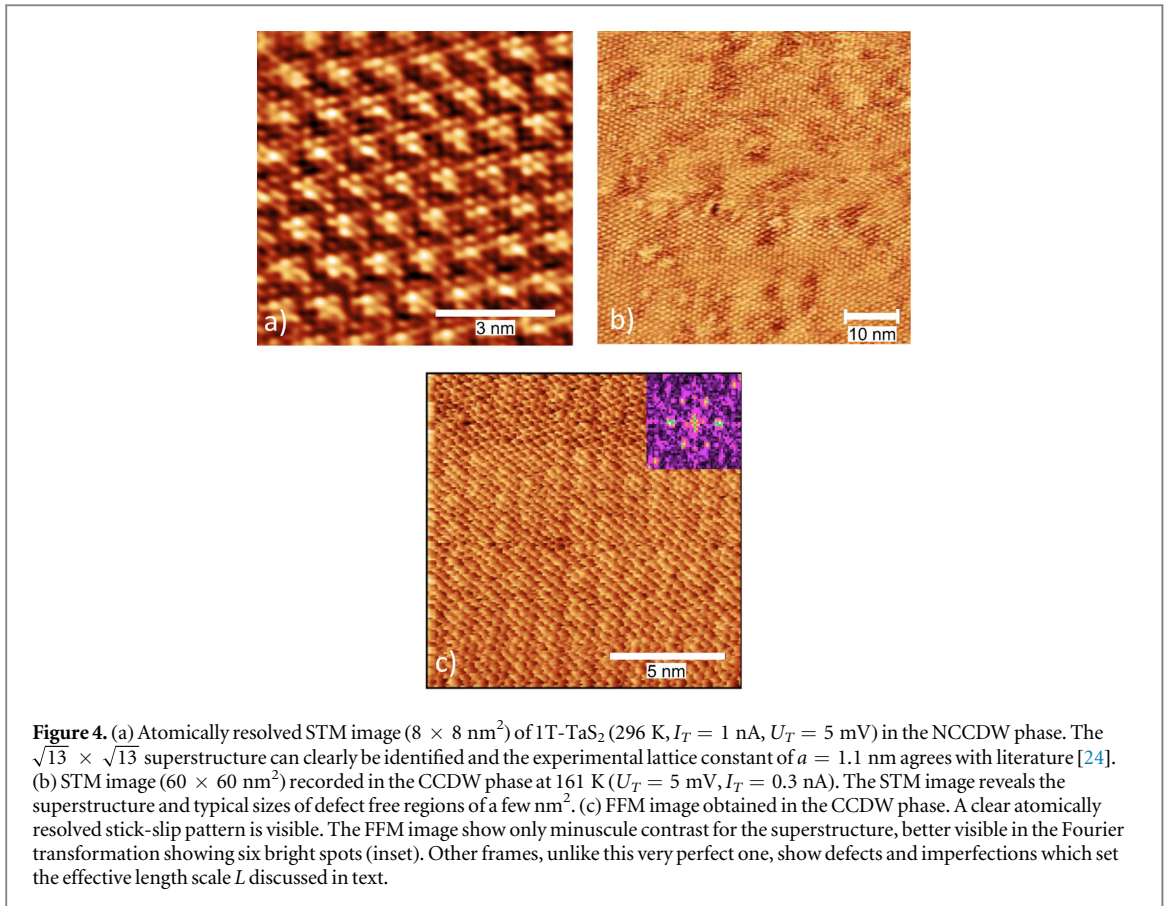
Experiment: AFM/FFM friction on 1T-TaS$_2$

Thus far the theory. To verify predictions in a well defined, physically interesting case we have chosen, as anticipated above, the CCDW–NCCDW transformation in the celebrated layer compound 1T-TaS$_2$, shown in figure 4. This is a thermally driven structural transition with an established and hysteresis cycle between phases that do not differ too strongly from one another.

The NCCDW–CCDW transformation takes place reproducibly in a single stage near $T_{NC} \sim 173$ K upon cooling. Its reverse takes place in two stages, at $T_{CT} \sim 223$ K and $T_{TN} \sim 280$ K, upon heating. That very reproducible hysteresis pattern, partly reproduced from [7] in figure 5, suggests that T_{NC} and T_{CT} are, to a good approximation, spinodal points of 1T-TaS$_2$. The spinodal nature is strongly confirmed by very recent heat capacity data by Kratochvilova *et al*, [23] showing no anomaly at T_{NC} and T_{CT}, despite the large electrical and structural bulk transformations. The absence of a heat capacity anomaly at both T_{NC} and T_{CT} is natural because the spinodal transformation occurs, upon temperature cycling $\pm \Delta T$, only once, thus averaging all internal energy effects to zero after the first passage.

To begin with, we restrict here to bulk 1T-TaS$_2$ in equilibrium. Focusing for definiteness on the NCCDW $\leftrightarrow$ CCDW transition upon cooling, and consider the phenomena which we might expect in AFM/FFM friction measurements as temperature crosses that transition.

First, frictional heat dissipation into the substrate (phononic friction) could in principle differ in the two phases, because their structures, phonon spectra, mechanical compliances are, even if mildly, different—for
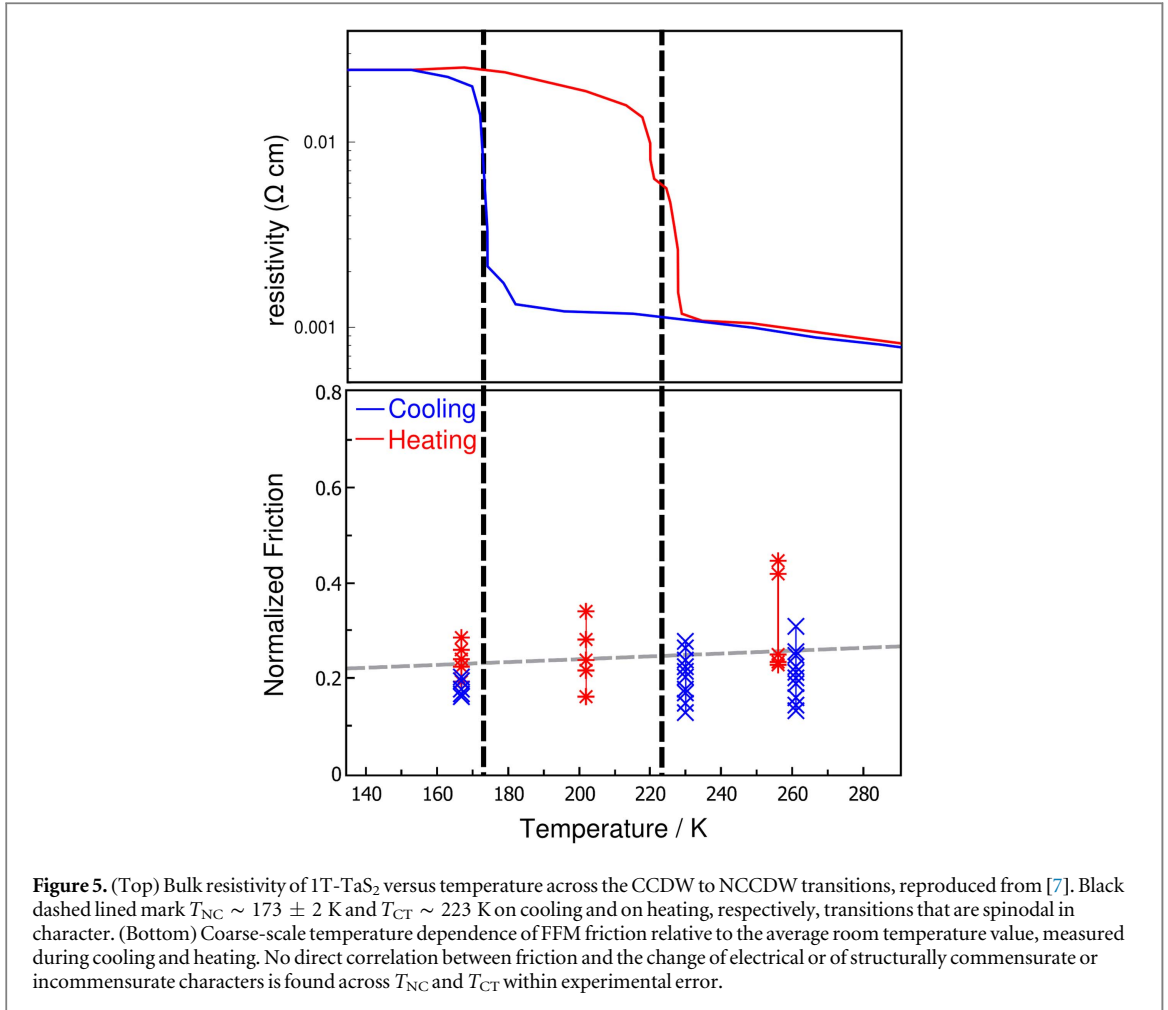
Figure 4. (a) Atomically resolved STM image (8×8 nm^2) of 1T-TaS$_2$ (296 K, $I_T = 1$ nA, $U_T = 5$ mV) in the NCCDW phase. The $\sqrt{13} \times \sqrt{13}$ superstructure can clearly be identified and the experimental lattice constant of $a = 1.1$ nm agrees with literature [24]. (b) STM image (60×60 nm^2) recorded in the CCDW phase at 161 K ($U_T = 5$ mV, $I_T = 0.3$ nA). The STM image reveals the superstructure and typical sizes of defect free regions of a few nm^2. (c) FFM image obtained in the CCDW phase. A clear atomically resolved stick-slip pattern is visible. The FFM image show only minuscule contrast for the superstructure, better visible in the Fourier transformation showing six bright spots (inset). Other frames, unlike this very perfect one, show defects and imperfections which set the effective length scale L discussed in text.

example, the NCCDW structure is known to possess a network of 'soliton' defects, absent in the CCDW. Second, electronic friction due to creation of electron–hole pairs could be present in the NCCDW phase which is metallic, and not in the CCDW which is insulating. Both mechanisms do suggest a higher non-contact friction in the higher temperature NCCDW phase than in the lower temperature CCDW phase. Our experiment however measures hard contact friction, where these contribution as we shall see turn out to be undetectable. The third, and central dissipation route described earlier is the main frictional feature which we observe near the spinodal points.

In our FFM experiments we used 1T-TaS$_2$-flakes with a size of approximately 4×4 mm^2 and a thickness before cleaving of about 50 μm. To yield clean surface conditions, the samples were freshly cleaved directly before transfer to the UHV chamber of a commercial Omicron-VT-AFM/STM system. Inside the UHV chamber the samples were additionally heated to 100 °C for 1 h to remove residual adsorbates from the surface. To ensure that the sample is apt to detect the anticipated effects, we first used high resolution STM imaging to identify the most characteristic feature related to the NCCDW and CCDW, namely the $\sqrt{13} \times \sqrt{13}$ superstructure formed by 13 Ta-atoms arranged in a star shape around a central atom [6]. This superstructure is revealed in figure 4(a), measured at 296 K. At this temperature, the superstructure forms separate hexagonal domains, which coalesce during the phase transformation on cooling, leading to CCDW 1T-TaS$_2$ [7].

Subsequently we use high resolution FFM for a first analysis of the sample with respect to tribological properties. Atomically resolved stick-slip is regularly observed and figure 4 (b) shows an example, which was measured in the CCDW phase at 173 K using a standard Si-cantilever (Nanosensors LFMR, normal force constant $k = 0.2$ N m^{-1}). Discerning the superstructure from the lateral force data in figure 4(b) is difficult and was only achieved for the CCDW phase by calculating the Fourier transform, where the superstructure leads to characteristic bright spots as shown in the inset of figure 4(b).

Starting from the 1T-TaS$_2$ surface, shown at room temperature in figure 4, we measure in the first experimental run, which serves as a coarse-scale reference, the temperature dependence of friction over a wide temperature range from room temperature down to 160 K. Figure 5 (bottom) shows that the friction remains constant within errors in the relevant range from 160 to 260 K. In particular there are no noticeable discontinuities across the spinodal transformation temperatures $T_{NC} \sim 173 \pm 2$ K and $T_{CT} \sim 223$ K indicated by the dashed lines. Also there is no difference or asymmetry between the cooling and heating cycles. One can see that incommensurability and metallization do not impact friction on this coarse scale. Much more detailed runs

Figure 5. (Top) Bulk resistivity of 1T-TaS$_2$ versus temperature across the CCDW to NCCDW transitions, reproduced from [7]. Black dashed lined mark $T_{NC} \sim 173 \pm 2$ K and $T_{CT} \sim 223$ K on cooling and on heating, respectively, transitions that are spinodal in character. (Bottom) Coarse-scale temperature dependence of FFM friction relative to the average room temperature value, measured during cooling and heating. No direct correlation between friction and the change of electrical or of structurally commensurate or incommensurate characters is found across T_{NC} and T_{CT} within experimental error.
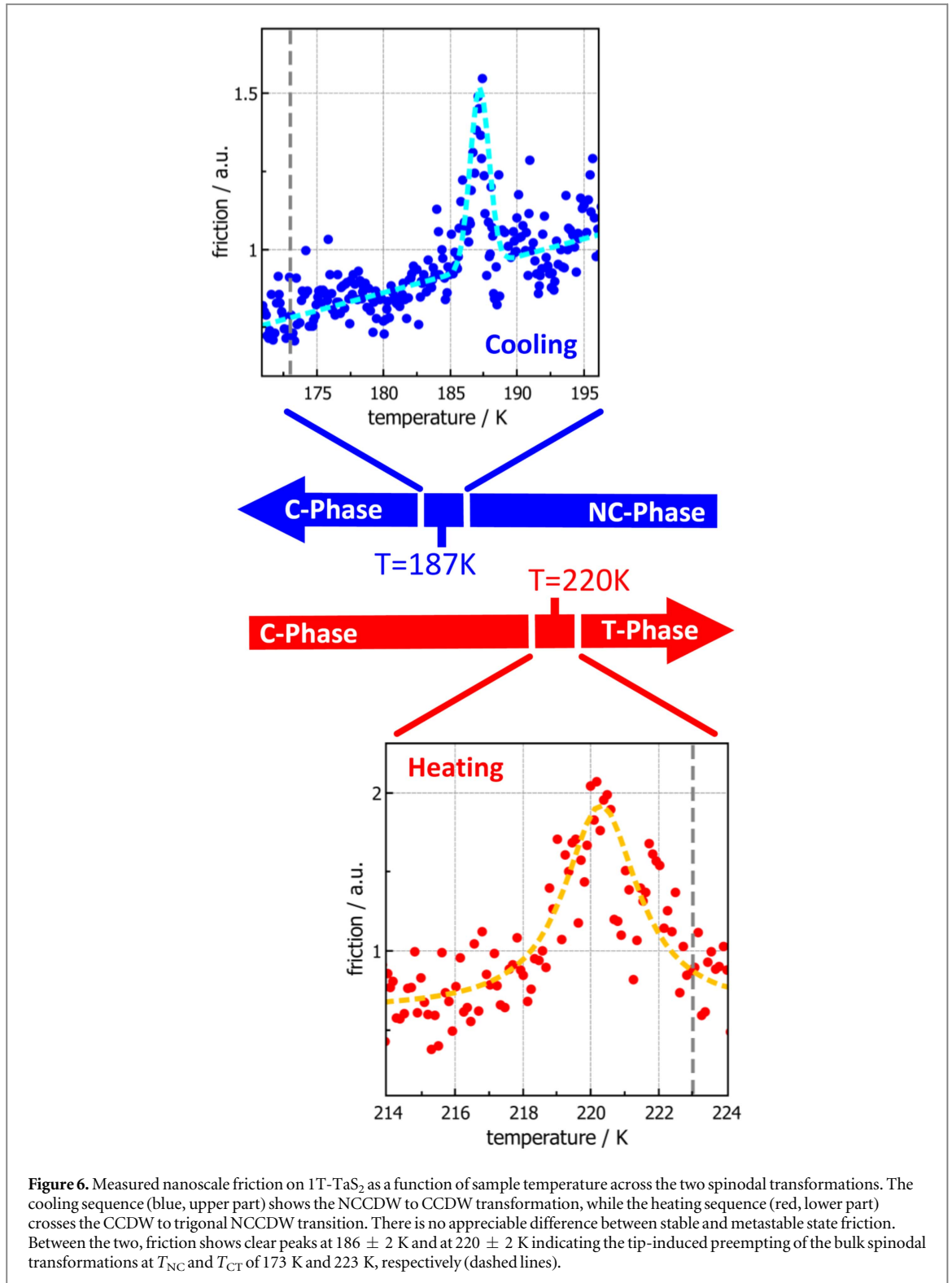
are necessary to discern the influence of the hysteretic (spinodal) transformations, present in structure and in conductivity, on the tip friction.

We subsequently focus on the friction signal in a much narrower temperature window around the anticipated spinodal transition points. We use a specific experimental protocol to measure lateral forces while crossing the transitions. First, the NCCDW to CCDW transformation is analyzed during cool down. For this the sample temperature was set to a constant value slightly above the transition point (appr. 195 K). Once a stable sample temperature is established, continuous scanning of FFM images with a size of 50×50 nm^2 at a normal force set-point of $F_N = 14$ nN and a scan speed of $v_{scan} = 250$ nm s^{-1} is started. Then the sample temperature is slowly reduced at a rate of appr. 0.2 K min^{-1} until the minimum temperature of 170 K is reached, while the scanning is continuously running with the normal force feedback enabled. The temperature change induces a z-drift of the sample, and therefore only a small temperature window of about 10–20 K is accessible with this method. Once the sample has been cooled down to the CCDW phase, the same procedure was used to analyze the transition from CCDW to NCCDW during heating. Here, 215 K was chosen as a starting point and the temperature was increased at a similar rate up to 225 K, thereby spanning the full phase transition.

For both cooling and heating sequences, the average friction force is calculated from each pair of lateral force images recorded for forward and backward scanning. Figure 6 shows the resulting friction during cooling and heating as a function of the simultaneously recorded temperature.

A clear peak in the average friction signal is now seen in both cooling and heating near the NCCDW–CCDW transformation temperatures. The peak height is approximately 1.5–2 times higher than the average friction signal away from the transition point, while the peak width is about 2–5 K. Results from further experiments reproduce these values. In contrast to published contact friction versus temperature results [25, 26], our result shows a very sharp and distinct transformation behavior, as qualitatively expected from the spinodal theory. It should be noted that in our experiments inducing the phase transition always required multiple scanning of the sample surface. This suggests, that inducing the phase transition must be considered as a statistical process, where surface defects and thermal activation are relevant. Additionally, the continuously changing temperature leads to lateral drift of the sample surface which thereby constantly provides new surface areas previously unaffected by the AFM-tip.

Figure 6. Measured nanoscale friction on 1T-TaS$_2$ as a function of sample temperature across the two spinodal transformations. The cooling sequence (blue, upper part) shows the NCCDW to CCDW transformation, while the heating sequence (red, lower part) crosses the CCDW to trigonal NCCDW transition. There is no appreciable difference between stable and metastable state friction. Between the two, friction shows clear peaks at 186 $\pm$ 2 K and at 220 $\pm$ 2 K indicating the tip-induced preempting of the bulk spinodal transformations at T_{NC} and T_{CT} of 173 K and 223 K, respectively (dashed lines).

Other details also fall qualitatively in place. The frictional peak on cooling occurs near 186 K, more than ten degrees higher than 173 $\pm$ 2 K, the tip-free bulk transformation, assumed to coincide with the spinodal temperature. This is precisely what our theory predicts, the temperature difference corresponding to $h_{\mathrm{c}} - h_{\mathrm{s}}$, a quantity in principle dependent on details including tip size and applied load. Moreover, comparison of heating and cooling frictional peaks shows that the heating peak deviates less from the bulk temperature $T_{\mathrm{CT}} \sim 223$ K. This is in agreement with a smaller difference expected in this case between Ψ_{m} and Ψ_{M}, reflecting the weaker character known for the transformation on heating relative to cooling [27]. The finite domain size L which limits the tip-triggered transformation in 1T-TaS$_2$ could be determined, besides the omnipresent defects shown in figure 4(c), also by the recently discovered interplanar mosaic structure of this material [28].

Discussion

We have proposed theoretically a mechanism predicting frictional anomalies at the spinodal points which end the hysteresis cycles of first-order phase transitions. Direct experimental demonstration of the anomaly is provided by FFM nanofriction measured at the two transformations which occur upon cooling (173 K) and upon heating (223 K) of the NCCDW ↔ CCDW transition of layered 1T-TaS$_2$, transformations which as heat capacity shows are to a good approximation spinodal in character. Near the spinodal temperature the free energy barrier protecting the metastable phase decreases enough that the small mechanical perturbation provided by the pressing and sliding tip is sufficient to locally trigger the transformation, thus preempting its spontaneous occurrence. The frictional anomaly predicted is transient, but can nonetheless be measured in steady sliding as the tip explores newer and newer untransformed areas. These results show that nanoscale friction, direct and easy to interpret, is as sensitive as resistivity or structural tools such as x-rays, unlike thermodynamic quantities like heat capacity that are totally insensitive when applied to spinodal points of first-order phase transitions. In the specific case of 1T-TaS$_2$, a possible interplay between the known electrical and structural characters of the transformations—characters which apparently do not impact the contact friction—and their spinodal nature, which we exploit here for the first time, will deserve renewed attention in the future. Of special interest appears to be for example the possibility to trigger tip-induced frictional transformations from hidden states generated under excitation [12], and/or in the ultrathin material, where the spinodal temperature is strongly thickness dependent [15]. Finally, we expect that a non-contact pendulum AFM experiment, [4] not yet tried to our knowledge in 1T-TaS$_2$, could yield relevant information on metallization and maybe on the presence or absence of a spinon gap in the CCDW Mott insulating phase.

Acknowledgments

ORCID iDs

Dirk Dietzel ⓘ https://orcid.org/0000-0001-6158-6971

References

[1] Vanossi A, Manini N, Urbakh M, Zapperi S and Tosatti E 2013 Colloquium: Modeling friction: from nanoscale to mesoscale *Rev. Mod. Phys.* **85** 529

[2] Benassi A, Vanossi A, Santoro G E and Tosatti E 2011 Sliding over a phase transition *Phys. Rev. Lett.* **106** 256102

[3] Kisiel M *et al* 2015 Noncontact atomic force microscope dissipation reveals a central peak of SrTiO$_3$ structural phase transition *Phys. Rev. Lett.* **115** 046101

[4] Kisiel M, Gnecco E, Gysin U, Marot L, Rast S and Meyer E 2011 Suppression of electronic friction on Nb films in the superconducting state *Nat. Mater.* **10** 119

[5] Binder K 1987 Theory of first-order phase transitions *Rep. Prog. Phys.* **50** 783

[6] Wilson J A, Di Salvo F and Mahajan S 1975 Charge-density waves and superlattices in the metallic layered transition metal dichalcogenides *Adv. Phys.* **24** 117–201

[7] Sipos B, Kusmartseva A F, Akrap A, Berger H, Forró L and Tutis E 2008 From Mott state to superconductivity in 1T-TaS$_2$ *Nat. Mater.* **7** 960

[8] Tosatti E and Fazekas P 1976 On the nature of the low-temperature phase of 1T-TaS$_2$, *J. Phys. Colloq.* **37** C4–165

[9] Fazekas P and Tosatti E 1979 Electrical, structural and magnetic properties of pure and doped 1T-TaS$_2$ *Phil. Mag.* B **39** 229–44

[10] Liu Y, Ang R, Lu W, Song W, Li L and Sun Y 2013 *Superconductivity induced by se-doping* in layered charge-density-wave system 1T-TaS$_{2-x}$Se$_x$ *Appl. Phys. Lett.* **102** 192602

[11] Perfetti L, Loukakos P, Lisowski M, Bovensiepen U, Berger H, Biermann S, Cornaglia P, Georges A and Wolf M 2006 Time evolution of the electronic structure of 1T-TaS$_2$ through the insulator–metal transition *Phys. Rev. Lett.* **97** 067402

[12] Stojchevska L, Vaskivskyi I, Mertelj T, Kusar P, Svetin D, Brazovskii S and Mihailovic D 2014 Ultrafast switching to a stable hidden quantum state in an electronic crystal *Science* **344** 177–80

[13] Laulhe C *et al* 2017 Ultrafast formation of a charge density wave state in 1T-TaS$_2$: observation at nanometer scales using time-resolved x-ray diffraction *Phys. Rev. Lett.* **118** 247401

[14] Yoshida M *et al* 2014 Controlling charge-density-wave states in nano-thick crystals of 1T-TaS$_2$ *Sci. Rep.* **4** 7302

[15] Yoshida M, Suzuki R, Zhang Y, Nakano M and Iwasa Y 2015 Memristive phase switching in two-dimensional 1T-TaS$_2$ crystals *Sci. Adv.* **1** e1500606

[16] Hovden R *et al* 2016 Atomic lattice disorder in charge-density-wave phases of exfoliated dichalcogenides (1T-TaS$_2$), *Proc. Natl Acad. Sci. USA* **113** 11420–4

[17] Zhao R *et al* 2017 Tuning phase transitions in 1T-TaS$_2$ via the substrate *Nano Lett.* **17** 3471–7

[18] Klanjšek M *et al* 2017 A high-temperature quantum spin liquid with polaron spins *Nat. Phys.* **13** 1130–4

[19] Law K T and Lee P A 2017 1T-TaS$_2$ as a quantum spin liquid *Proc. Natl Acad. Sci.* **114** 6996–7000

[20] Ribak A, Silber I, Baines C, Chashka K, Salman Z, Dagan Y and Kanigel A 2017 Gapless excitations in the ground state of 1T-TaS$_2$ *Phys. Rev. B* **96** 195131

[21] Langer J S 1967 Theory of the condensation point *Ann. Phys., NY* **41** 108–57

[22] Cahn J and Allen S 1977 A microscopic theory for domain wall motion and its experimental verification in Fe–Al alloy domain growth kinetics *J. Phys. Colloq.* **38** C7–51

[23] Kratochvilova M, Hillier A D, Wildes A R, Wang L, Cheong S-W and Park J-G 2017 The low-temperature highly correlated quantum phase in the charge-density-TaS$_2$ compound *npj Quantum Mater.* **2** 42

[24] Thomson R E, Burk B, Zettl A and Clarke J 1994 Scanning tunneling microscopy of the charge-density-wave structure in 1T-TaS$_2$ *Phys. Rev. B* **49** 16899–916

[25] Jansen L, Schirmeisen A, Hedrick J L, Lantz M A, Knoll A, Cannara R and Gotsmann B 2009 Nanoscale frictional dissipation into shear-stressed polymer relaxations *Phys. Rev. Lett.* **102** 236101

[26] Jansen L, Lantz M A, Knoll A W, Schirmeisen A and Gotsmann B 2014 Frictional dissipation in a polymer bilayer system *Langmuir* **30** 1557–65

[27] Guy D, Ghorayeb A, Bayliss S and Friend R 1985 High pressure investigation of the CDW phase diagram of 1T-TaS$_2$ *Charge Density Waves in Solids* (Berlin: Springer) pp 80–3

[28] Ma L *et al* 2016 A metallic mosaic phase and the origin of Mott-insulating state in 1T-TaS$_2$ *Nat. Commun.* **7** 10956